

Insights into the heavy dense QCD phase diagram using Complex Langevin simulations

Gert Aarts¹, Felipe Attanasio^{1,2}, Benjamin Jäger^{*1}, Erhard Seiler³, Dénes Sexty⁴, Ion-Olimpiu Stamatescu⁵.

¹*Department of Physics, College of Science, Swansea University, Swansea, UK*

²*CAPES Foundation, Ministry of Education of Brazil, Brasília, Brazil*

³*Max-Planck-Institut für Physik (Werner-Heisenberg-Institut), München, Germany*

⁴*Department of Physics, Bergische Universität Wuppertal, Wuppertal, Germany*

⁵*Institut für Theoretische Physik, Universität Heidelberg, Heidelberg, Germany*

E-mail: B.Jaeger@swansea.ac.uk

Complex Langevin simulations provide an alternative to sample path integrals with complex weights and therefore are suited to determine the phase diagram of QCD from first principles. Adaptive step-size scaling and gauge cooling are used to improve the convergence of our simulations. We present results for the phase diagram of QCD in the limit of heavy quarks and discuss the order of the phase transitions, which are studied by varying the spatial simulation volume.

*The 33rd International Symposium on Lattice Field Theory
14 - 18 July 2015
Kobe International Conference Center, Kobe, Japan*

*Speaker.

1. Introduction

Complex Langevin simulations [1-4] have recently become an active field of research with the development of *gauge cooling* [5,6] and the prospect of enabling studies of QCD with non-vanishing chemical potential [7]. Here we report on our ongoing project studying the phase diagram of QCD. A sketch of the expected phase diagram for QCD is shown in Figure 1. First principle calculations are a crucial input for understanding the behaviour of strong interactions in heavy ion collisions and in neutron stars.

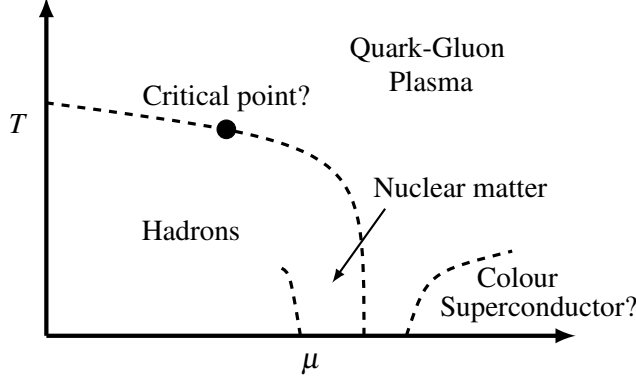


Figure 1: A scenario of the QCD phase diagram.

Before studying the QCD phase diagram of full QCD, we consider the heavy dense approximation of QCD (HDQCD) [4, 5, 8] as a first test and identify the necessary step to determine the location and order of the phase transitions. Currently, we do not consider higher orders in the hopping parameter expansion, as done in [9-11], since our final goal is to study QCD with fully dynamical light quarks.

2. Complex Langevin simulation

Complex Langevin simulations are based on a stochastic process, which is achieved by an update using simple matrix multiplication

$$U_{\mu x}(t + \varepsilon) = R(t) U_{\mu x}(t). \quad (2.1)$$

The update matrix is composed of a deterministic drift and a stochastic term, and can be written as

$$R(t) = \exp [i\lambda (-\varepsilon D_U S + \sqrt{\varepsilon} \eta)], \quad (2.2)$$

where λ are the Gell-Mann matrices of SU(3) and $D_U S$ is the gauge derivative of the action. The stochastic part is provided by Gaussian white noise η . We use Wilson's plaquette action in the gauge sector and include fermions by the logarithm of the fermion determinant, which in the limit of heavy quarks can be written for one flavour as

$$\det D(\mu) = \prod_{\vec{x}} \det \left(1 + h e^{\mu/T} \mathcal{P}_{\vec{x}} \right)^2 \det \left(1 + h e^{-\mu/T} \mathcal{P}_{\vec{x}}^{-1} \right)^2 \quad (2.3)$$

with $h = (2\kappa)^{N_\tau}$. Recent work [12-15] has shown that the complex logarithm does not necessarily spoil Complex Langevin dynamics, as long as the quark masses are sufficiently large. Due to the complex nature of the QCD path integral in the presence of finite quark density, the gauge links are an element of the gauge group $SL(3, \mathbb{C})$. We use adaptive step-size scaling [16] and adaptive gauge cooling [5, 6] to avoid large excursions into the non-compact extension of $SU(3)$, which would invalidate the justification of the approach [17, 18]. To check our simulations, we monitor the 'unitnorm' during the Langevin evolution,

$$d = \text{Tr} (UU^\dagger - \mathbb{I})^2, \quad (2.4)$$

which is a measure of the distance to the $SU(3)$ manifold and a good indicator of stability of our runs.

3. Numerical setup

We study the phase diagram of heavy dense QCD using two flavours of heavy quarks and work at a fixed lattice spacing (fixed β). To improve our previous results [19, 20] we have extended our simulations to cover two additional spatial volumes, i.e. 6^3 and 10^3 . We perform a simultaneous scan in the chemical potential and the temperature by varying μ and N_τ . The range of our simulation parameter can be found in Table 1. Our simulations have been extended to a maximum

$\beta = 5.8$	$N_f = 2$	$V = 6^3, 8^3, 10^3$
$\kappa = 0.04$	$\mu = 0.0 - 3.2$	$N_\tau = 2 - 32$
	$a \sim 0.15 \text{ fm}$	$T = 670 - 42 \text{ MeV}$

Table 1: Summary of simulation parameters, where the chemical potential is given in lattice units. The lattice spacing has been determined using the Wilson flow in [7, 21].

Langevin time of 500, of which we discarded the first 100 to remove thermalisation effects. We use a step-size of $\varepsilon \sim 10^{-4}$ and apply adaptive step-size scaling to compensate for large forces in the Langevin drifts. We determine observables every 10^{-2} Langevin time. Configurations are typically decorrelated when separated by approximately 10 – 100 measurements, depending on the actual value of the spatial volume, chemical potential and temperature. For each setup we have at least 4000 – 400 decorrelated configurations. The auto-correlation has been determined using the algorithm described in [22].

4. Results

Figure 2 shows the result for the Polyakov loop as a function of temperature T and the chemical potential μ for the spatial volume of 8^3 . The temperature axis is shown in units of MeV using the lattice spacing of $a \sim 0.15 \text{ fm}$, which has been obtained using the Wilson flow [7, 21]. The chemical potential is shown in units of the quark mass, which for HDQCD can be simply written as

$$m_q \equiv -\ln(2\kappa) = 2.53 \sim \mu_c. \quad (4.1)$$

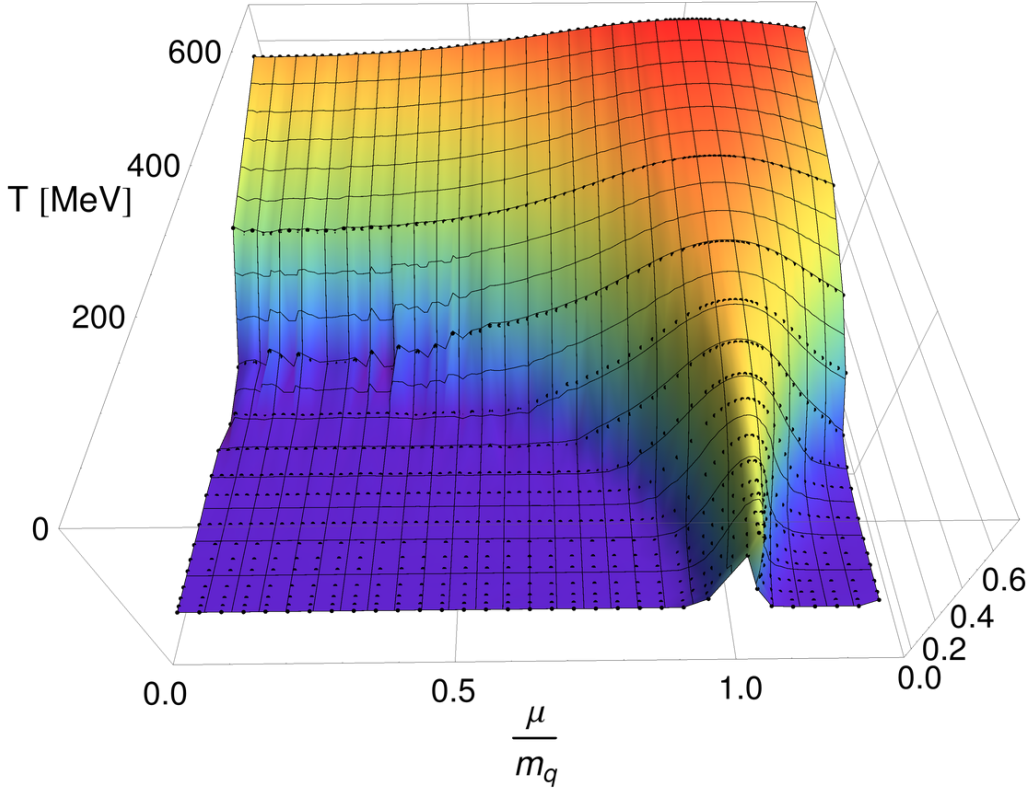


Figure 2: The Polyakov loop as function of temperature T and chemical potential μ for the 8^3 ensembles. Each black dot represent the result of a Complex Langevin simulation.

The expected critical chemical potential μ_c is directly related to the quark mass in the heavy dense approximation of QCD. The Polyakov loop is an excellent quantity to study both transitions, i.e. the deconfinement transition and the transition to higher densities. An intrinsic lattice artefact is visible at large chemical potentials, which can be understood by Pauli blocking. At high enough densities all lattice sites are filled with fermions and no additional fermion can be added. The Polyakov loop drops to zero in this unphysical regime, since the system is effectively equivalent to a pure gauge. The fermion density on the other hand shows saturation for high densities. Figure 2 also shows a cubic interpolation of the data, represented by the coloured surface connecting the individual results to guide the eye. Figure 3 shows the equivalent plot for the Polyakov loop susceptibility as a function of μ and T for our intermediate volume of 8^3 . This plot provides a good representation of the phase boundary of HDQCD. The broadness seen for the deconfinement transition is caused by the limited resolution in the temperature direction, since the temporal extent is naturally an integer. Varying the gauge coupling and thereby the lattice spacing will allow us to probe different temperatures and study also the behaviour towards the continuum limit.

To study the transitions in more detail, we have simulated HDQCD with three different volumes, i.e. $6^3, 8^3$ and 10^3 . Figure 4 shows the susceptibility of the fermion density n , where the latter is defined as

$$n = \frac{1}{N_\tau N_s^3} \frac{\partial \ln Z}{\partial \mu}. \quad (4.2)$$

The fermion density and its susceptibility provide a very clear signal for the transition to higher

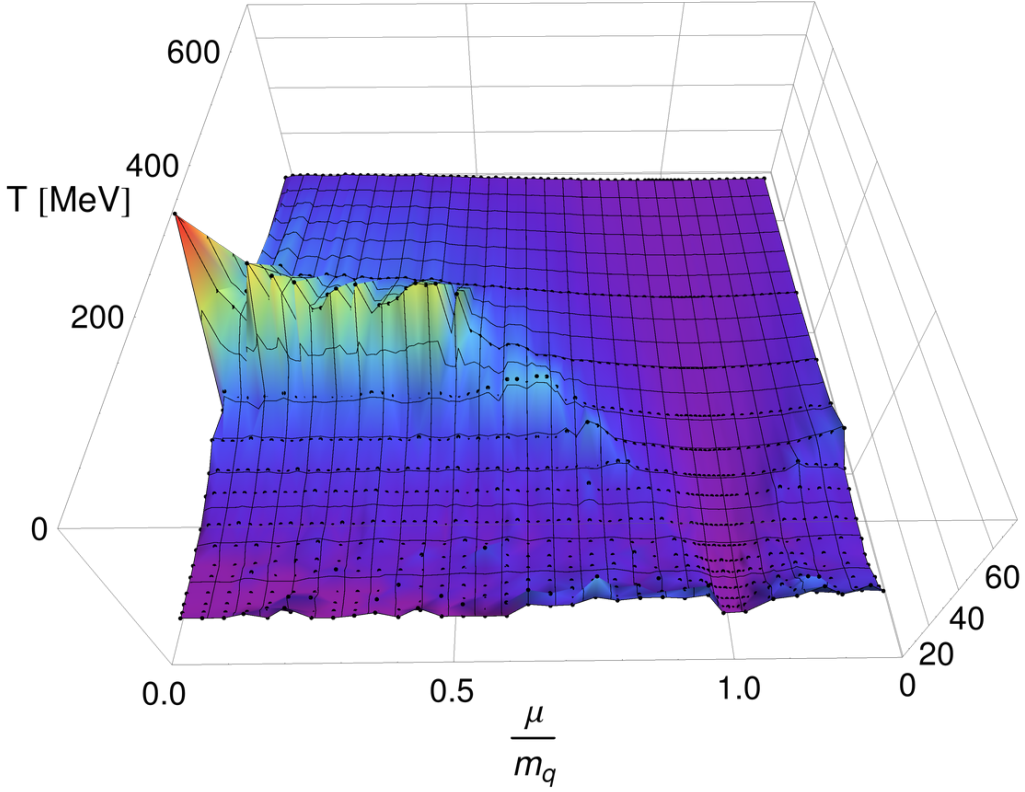


Figure 3: The Polyakov loop susceptibility as function of T and μ in the same style as Figure 2.

densities. An approximate symmetry is visible in Figure 4 around the critical chemical potential μ_c , which can be understood by considering a symmetry between particles and holes [23]. At half-filling, which is reached at μ_c , the susceptibility drops and shows a symmetric behaviour on both sides within statistical fluctuations. The upper panel of Figure 4 depicts the transition for one of our larger temperatures of $T \sim 335$ MeV, whereas the lower panel shows the situation for a smaller temperatures of $T \sim 167$ MeV.

5. Conclusions and Outlook

Here we presented an update of our ongoing project to study the phase diagram of (heavy dense) QCD from first principles using Complex Langevin simulations. We find clear signals for the deconfinement transition and the transition to higher density. Currently, we are extending our simulations to even larger volumes around the transition, to better identify the order of the transitions. Varying the gauge coupling will allow us to improve the resolution of the deconfinement transition and study the continuum limit. With this study we have presented the necessary steps and methods to study the phase diagram of fully dynamical QCD using staggered quarks [7], which we plan to study next.

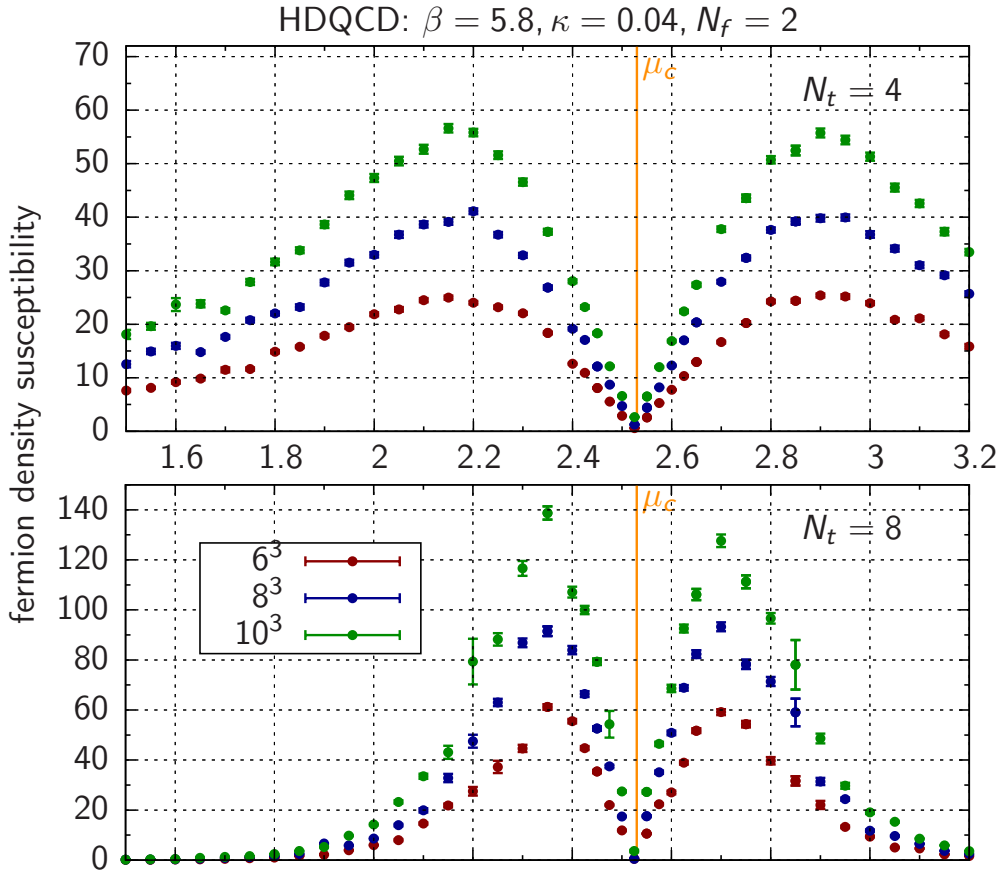


Figure 4: The fermion density susceptibility as a function of the chemical potential for two different temporal extents $N_t = 4$ (upper) and $N_t = 8$ (lower). The volumes are shown in different colours.

Acknowledgements: We are grateful for the computing resources made available by HPC Wales. Part of this work used the DiRAC BlueGene/Q Shared Petaflop system at the University of Edinburgh, operated by the Edinburgh Parallel Computing Centre on behalf of the STFC DiRAC HPC Facility (www.dirac.ac.uk). This equipment was funded by BIS National E-infrastructure capital grant ST/K000411/1, STFC capital grant ST/H008845/1, and STFC DiRAC Operations grants ST/K005804/1 and ST/K005790/1. DiRAC is part of the National E-Infrastructure. We acknowledge the STFC grant ST/L000369/1, the Royal Society and the Wolfson Foundation. FA is grateful for the support through the Brazilian government programme “Science without Borders” under scholarship number BEX 9463/13-5.

References

- [1] G. Parisi, Phys. Lett. B **131** (1983) 393.
- [2] J. R. Klauder, Acta Phys. Austriaca Suppl. **25** (1983) 251.
- [3] J. R. Klauder, Phys. Rev. A **29** (1984) 2036.
- [4] G. Aarts and I. O. Stamatescu, JHEP **0809** (2008) 018.

- [5] E. Seiler, D. Sexty and I. O. Stamatescu, Phys. Lett. B **723** (2013) 213.
- [6] G. Aarts, L. Bongiovanni, E. Seiler, D. Sexty and I. O. Stamatescu, Eur. Phys. J. A **49** (2013) 89.
- [7] D. Sexty, Phys. Lett. B **729** (2014) 108.
- [8] I. Bender, T. Hashimoto, F. Karsch, V. Linke, A. Nakamura, *et al.*, Nucl. Phys. Proc. Suppl. **26** (1992) 323.
- [9] R. De Pietri, A. Feo, E. Seiler and I. O. Stamatescu, Phys. Rev. D **76** (2007) 114501
- [10] M. Fromm, J. Langelage, S. Lottini and O. Philipsen, JHEP **1201** (2012) 042
- [11] G. Aarts, E. Seiler, D. Sexty and I. O. Stamatescu, Phys. Rev. D **90** (2014) 11, 114505
- [12] A. Mollgaard and K. Splittorff, Phys. Rev. D **88** (2013) 11, 116007
- [13] K. Splittorff, Phys. Rev. D **91** (2015) 3, 034507
- [14] J. Nishimura and S. Shimasaki, Phys. Rev. D **92** (2015) 1, 011501
- [15] J. Greensite, Phys. Rev. D **90** (2014) 11, 114507
- [16] G. Aarts, E. Seiler and I. O. Stamatescu, Phys. Rev. D **81** (2010) 054508.
- [17] G. Aarts, F. A. James, E. Seiler and I. O. Stamatescu, Eur. Phys. J. C **71** (2011) 1756.
- [18] G. Aarts, F. A. James, E. Seiler and I. O. Stamatescu, Phys. Lett. B **687** (2010) 154.
- [19] G. Aarts, F. Attanasio, B. Jäger, E. Seiler, D. Sexty and I. O. Stamatescu, PoS LATTICE **2014** (2014) 200
- [20] G. Aarts, F. Attanasio, B. Jäger, E. Seiler, D. Sexty and I. O. Stamatescu, Acta Phys. Polon. Supp. **8** (2015) 2, 405
- [21] S. Borsanyi, S. Durr, Z. Fodor, C. Hoelbling, S. D. Katz, *et al.*, JHEP **1209** (2012) 010.
- [22] U. Wolff [ALPHA Collaboration], Comput. Phys. Commun. **156** (2004) 143 [Comput. Phys. Commun. **176** (2007) 383]
- [23] T. Rindlisbacher and P. de Forcrand, arXiv:1509.00087 [hep-lat].